To What Extent Biomass Burning Aerosols Impact South America Seasonal Climate Predictions?

Julliana L. M. Freire[1] [iD], **Karla M. Longo[2,3], Saulo R. Freitas[2,3]** [iD], **Caio A. S. Coelho[1]**, **Andrea M. Molod[3], Jelena Marshak[3], Arlindo da Silva[3]**, and **Bruno Z. Ribeiro[4]** [iD]

[1]Center for Weather Forecast and Climate Studies, National Institute for Space Research, Cachoeira Paulista, SP, Brazil, [2]Universities Space Research Association, Columbia, MD, USA, [3]NASA Goddard Space Flight Center, Greenbelt, MD, USA, [4]Department of Atmospheric and Environmental Sciences, University at Albany, Albany, NY, USA

Abstract We applied the Goddard Earth Observing System for subseasonal to seasonal climate prediction to assess the impact of inclusion biomass burning (BB) aerosols over South America (SA) during the austral winter. We also evaluated the model sensitivity to the BB emissions prescription using no emissions, monthly climatological, and daily emissions. Each hindcast consisted of four members running from June to November of each year between 2000 and 2015. Our results indicated that interactive BB aerosols improve the seasonal climate prediction performance over SA. More realistic daily based emissions significantly further improve the performance in comparison with the climatological ones. Therefore, improvements in the BB emissions representation are urged to represent the aerosol impacts on seasonal climate prediction performance adequately.

Plain Language Summary Vegetation fires severely affect tropical forest and savannah-type biomes in South America (SA) during winter in Southern Hemisphere. Biomass burning (BB) aerosols are important agents changing energy budget and clouds. This study focused on assessing whether including aerosol-radiation-cloud interaction in a climate model, particularly the contribution of BB aerosols, can provide additional information for improving seasonal climate predictions. This study has two primary outcomes. First, that including BB aerosols does improve the model's ability to predicted precipitation and near-surface temperature in SA. Second, it proved it is indeed essential to improve BB emissions representation to further elevate seasonal climate prediction performance.

1. Introduction

Coupled ocean–atmosphere–land–ice numerical modeling systems are the state of the art in climate forecasting, aggregating the best and most up-to-date scientific knowledge. Oceanic conditions are recognized as the most critical seasonal climate forcing in these systems. In the past decades, seasonal forecasting reached a high level of development, mainly due to advances in understanding the dynamics of the El Niño–Southern Oscillation (ENSO) phenomenon (Doblas-Reyes et al., 2013), which was the primary source of predictability on the seasonal time scale. These advances were possible mostly due to the use of remote sensing and buoys to monitor the sea surface temperature (SST) and atmospheric conditions, the development of physically based numerical models to predict the joint ocean–atmosphere evolution, and the implementation of multimodel ensemble techniques. Nowadays, the seasonal climate forecast performance is mostly affected by model errors related to the climate model itself, which include lack or misrepresentation of some physical processes. More recently the scientific community has been exploring the sensitivity of climate forecasting to new climate system forcings, such as changes in land use, and concentration of radiative gases and aerosols in the atmosphere to improvement in quality the climate predictions (Doblas-Reyes et al., 2013; Kirtman & Pirani, 2009).

In South America (SA), the typical dry austral winter and countries' policies for expanding the agricultural/pasture frontiers toward the Tropical Forest and Cerrado biomes have been in place for decades, contributed to defining the so-called biomass burning (BB) season in the region. Extensive vegetation fire activity related to deforestation and land use management, usually lasting for at least 3 months every year, releases a considerable amount of smoke to the atmosphere. The aerosol particles produced by BB activities contribute to at least 90% of the total aerosol optical depth (AOD) in the visible spectrum, which jumps from

the average range from 0.2 to 0.4 up to values 10 times higher over several million square kilometers (Rosário et al., 2013). Modeling studies indicate a surface cooling of up to 3°C in Amazonia associated with the aerosols-radiation interaction, limiting the turbulent mixing and, consequently, the evapotranspiration and sensible heat flux. This leads to a drier and shallower planetary boundary layer (PBL) that acts to inhibit the formation and development of convective clouds and precipitation (Yu et al., 2002). Moreover, BB aerosols with sufficiently high supersaturation relative to water vapor, despite their typically low to moderate hygroscopicity, can efficiently act as cloud condensation nuclei (Gácita et al., 2017), therefore modifying cloud microphysical properties and dynamics.

Furthermore, modeling studies suggest that the induced aerosol changes in near surface and the troposphere temperatures impact global circulation patterns, affecting the strength of the Hadley cell (Allen et al., 2012a, Allen et al., 2012, Tosca et al., 2013). Randles et al. (2013) showed that during the austral winter, the high loading of BB aerosols in the atmosphere strengthens the descending branch of Hadley circulation in the tropics (around 30°S) and weakens the ascending branch around 15°N.

Benedetti and Vitart (2018) showed the potential for the use of interactive prognostic aerosols to improve predictions at the subseasonal scales. Including prognostic aerosol interactions in the European Centre for Medium-Range Forecasts (ECMWFs) model reduced the temperature and wind biases over several areas in the tropics and midlatitudes. They also showed a significant positive impact of the prognostic aerosols on several meteorological fields, including upper-level winds and lower-tropospheric temperatures, particularly over the Northern Hemisphere. In addition to these rapid changes due to aerosol-radiation-cloud interactions, the relatively slow response to SST changes is also critically important for atmospheric circulation and, consequently, for the tropical rainfall patterns (Andrews et al., 2009; He & Soden, 2015). Responses mediated by SST due to aerosol forcing play an important role in monsoon rainfall patterns, which are predominantly controlled by SST anomalies (Li et al., 2020; Ma & Xie, 2013; Wang et al., 2016).

It is well-established that the net aerosol forcing translates into changes in energy fluxes between the atmosphere and the Earth's surface, which ultimately affects even the global atmospheric circulation and thermodynamic profile. However, climate prediction of BB emissions in SA is still a challenging subject as its controlling factors include natural climate phenomena, such as ENSO, as well as strong social-economic forcing. This study aims to contribute to this scientific debate by addressing the following questions: What is the impact of explicitly including BB aerosol forcing in a seasonal forecast climate model in terms of forecast performance and representation of the seasonal climatological features, especially over SA? What is the sensitivity of the seasonal climate to the temporal resolution of BB emissions?

2. Methods and Data

2.1. GEOS-S2S-2.1 System

We applied the version 5 of the Goddard Earth Observing System (GEOS) global circulation model (GCM) for subseasonal to seasonal climate prediction (GEOS-S2S-2, Molod et al., 2020). The GEOS-S2S-2 includes a coupled Atmosphere–Ocean GCM (AOGCM), an ocean data assimilation system (ODAS), and a methodology for weakly coupled Atmosphere–Ocean Coupled Data Assimilation (AODAS). Text S1 (support information, SI) provides further details about the GEOS modeling system version here applied.

The GEOS simulated radiative transfer through the atmosphere considers the presence of aerosols by calculating the scattering and absorbing solar radiation as a function of aerosol intrinsic properties and concentration in the atmospheric column. The longwave and shortwave radiative schemes follow Chou and Suarez (1994) and Chou (1990, 1992), respectively. The two-moment cloud microphysics includes the indirect effect of aerosol on clouds, considering the activation of aerosol particles as both cloud condensation nuclei (CCN) and ice nuclei (IN) explicitly. The CCN activation follows the Fountoukis and Nenes (2005) approach, which gives an analytical solution of the equations of an adiabatic ascending cloudy parcel (Nenes & Seinfeld, 2003). The IN activation also resolves the equations for an ascending adiabatic air parcel (Barahona & Nenes, 2008, 2009), considering both the homogeneous (Koop et al., 2000) and heterogeneous (Phillips et al., 2013) activation. Additional details of how the indirect effect works in the GEOS-S2S system can be found in Barahona et al. (2014). Furthermore, the oceanic model, coupled with the atmospheric model, simultaneously predicts the SST, which is the variable that exerts the most vigorous control over
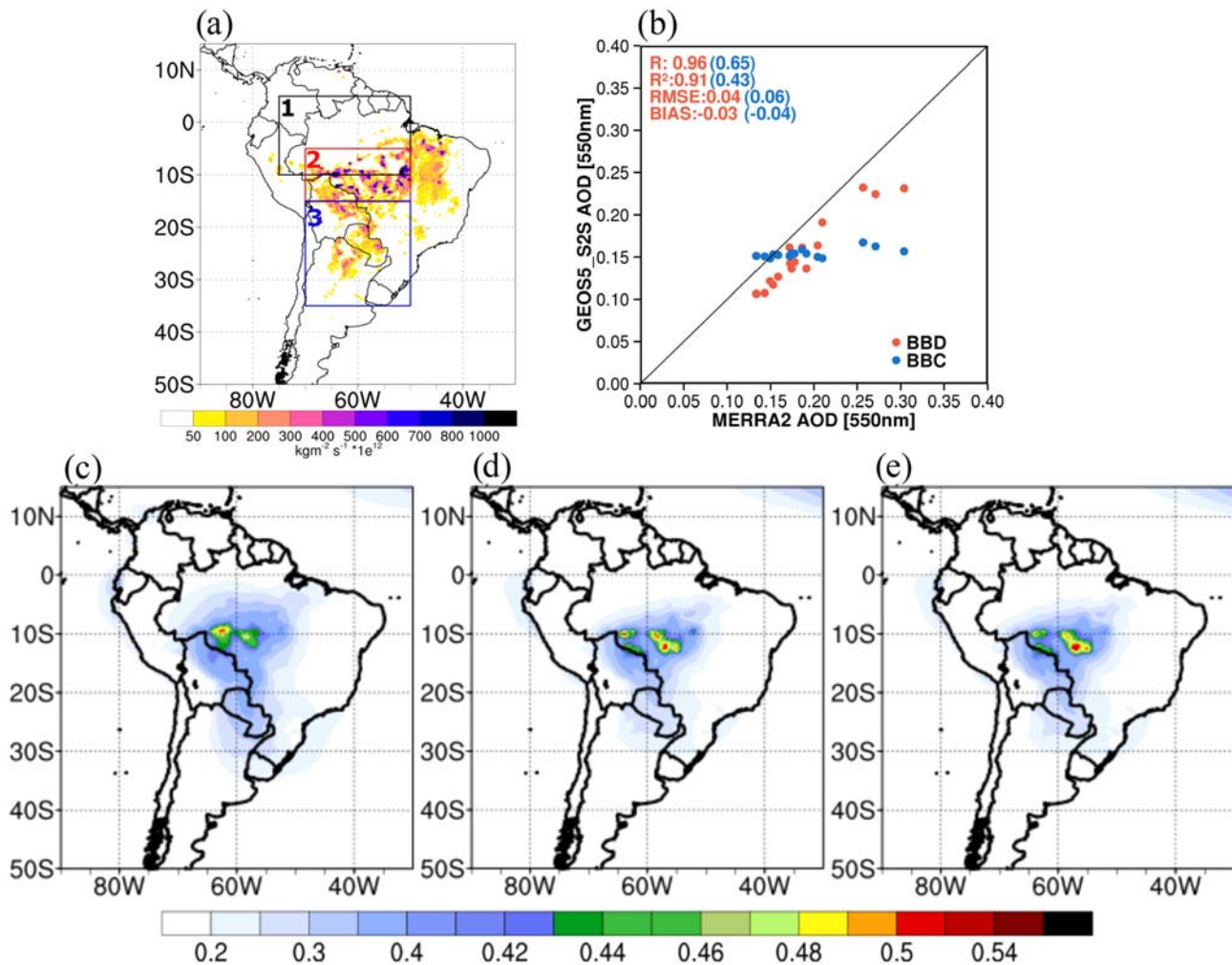
Figure 1. (a) Climatological mean (2000–2015) spatial distribution of the BB emissions during the trimester August–October (ASO), based on the QFED inventory; (b) scatterplot of the annually ASO mean AOD values over SA from MERRA-2 and the models results from BBC and BBD for the period 2000–2015. Spatial distribution of the ASO climatological mean (2000–2015) AOD (550 nm) for (c) MERRA-2, (d) BBC, and (e) BBD model runs. The rectangles in the map in (a) indicate regions 1 (black), 2 (red), and 3 (blue), details on the text.

the circulation and precipitation patterns on the SA, mainly through the effects of ENSO, therefore accounting for any changes in the SST due to aerosol forcing.

2.2. Aerosol Emissions

Text S2 (SI) summarizes the emissions from several sources and for the various types of aerosols included in GOCART, the GEOS aerosol component. Figure S1 (SI) depicts the climatology of BB aerosol emissions in SA, peaking around 21 $kgm^{-2}s^{-1} \times 10^{-12}$ in September and its monthly mean annual variability from 2000 to 2015, based on the Quick Fire Emission Dataset (QFED) inventory version 2.5 (Darmenov & da Silva, 2015). Figure 1a shows that the mean spatial distribution of these emissions over SA. Despite the clear seasonality, the apex of BB emissions in SA varies from 10 $kgm^{-2}s^{-1} \times 10^{-12}$ to almost four times higher between August and September.

2.3. Remote Sensing and Reanalysis Data Sets for Model Evaluation

We used the monthly Tropical Rainfall Measuring Mission (TRMM; Simpson et al., 1996) 3B43 precipitation product to evaluate our model precipitation results. As a reference for the evaluation of all other variables, we used the Modern-Era Retrospective analysis for Research and Applications, Version 2 (MERRA-2; Gelaro et al., 2017, Randles et al., 2017). Text S3 (SI) has detailed information about MERRA-2 and TRMM.
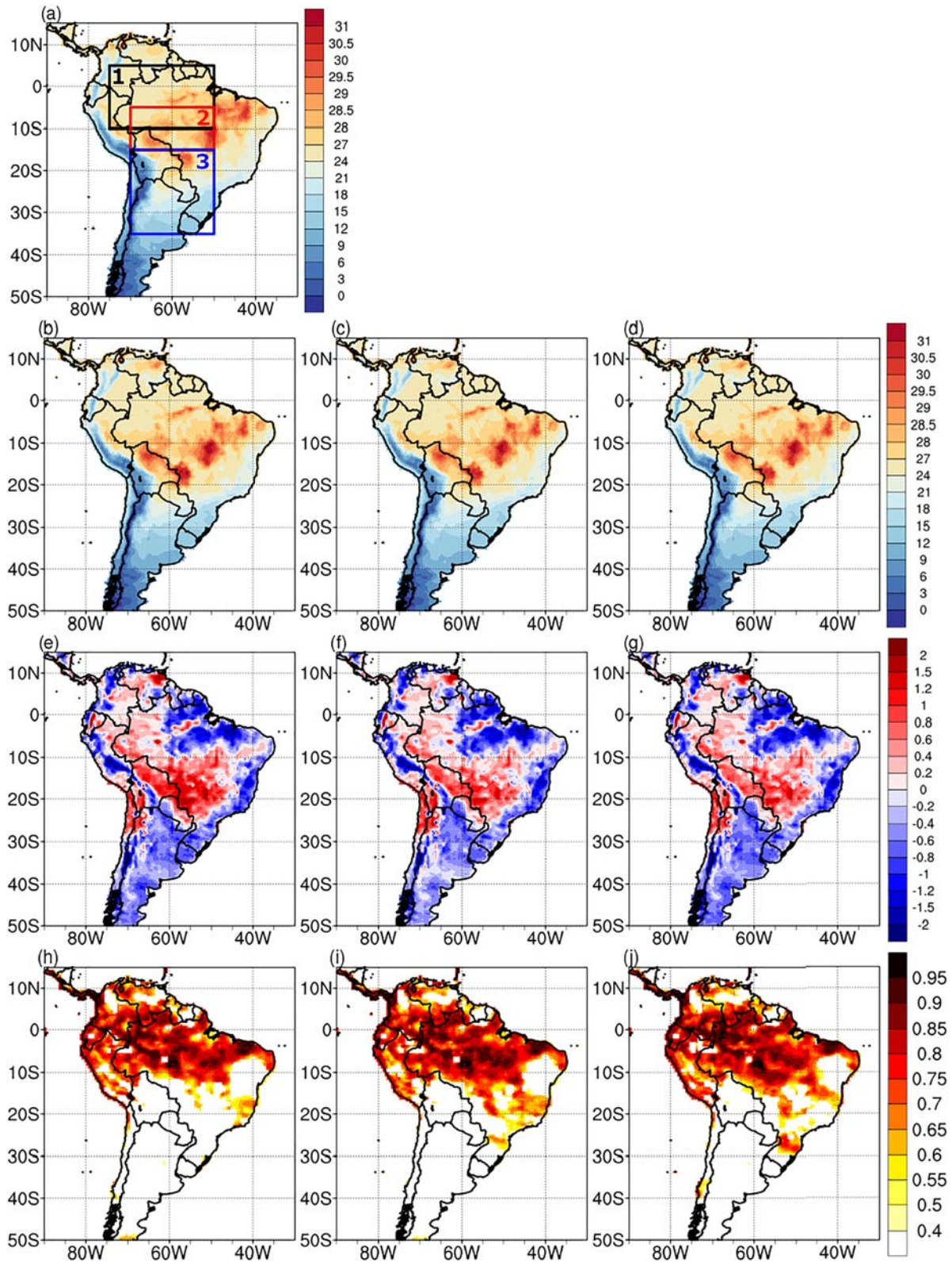
Figure 2. Climatological mean ASO spatial distribution (2000–2015) of 2-m temperature (°C) from (a) MERRA-2, (b) BBZ, (c) BBC, and (d) BBD. Mean bias of 2-m temperature from GEOS-S2S-2 relative to MERRA-2 for (e) BBZ, (f) BBC, and (g) BBD experiments. Correlation between 2-m temperature anomaly from GEOS-S2S-2 and the corresponding MERRA-2 for (h) BBZ, (i) BBC, and (j) BBD experiments. The correlation plots show only the points with 5%SSL using a two-sided Student's *t* test.

Table 1
Correlation (R), Bias, and Mean Square Root Error (RMSE) Computed for 2-m Temperature (°C) Predicted Anomalies and MERRA-2 Over the Regions 1–3 From All Three Experiments

	Region 1 (10°S–5°N;75–50 W)			Region 2 (15–5°S;70–50 W)			Region 3 (35–15°S;65–45 W)		
	R	Bias	RMSE	*R*	Bias	RMSE	*R*	Bias	RMSE
BBZ	0.78	−0.12	0.71	0.64	0.21	0.99	0.55	0.08	1.42
BBC	0.80	−0.19	0.69	0.72	0.04	0.93	0.62	−0.01	1.46
BBD	0.80	−0.17	0.70	0.73	0.07	0.96	0.61	−0.04	1.45

*Note.* The regions are depicted in Figure 2a.

2.4. Experimental Design

GEOS-S2S-2 was run with $0.5° \times 0.5°$ spatial resolution and 72 vertical levels, extending from the surface to 0.01 hPa, resolving both the troposphere and the stratosphere. The MERRA-2 data was used for model initialization. We carried out three experiments to assess the role played by BB aerosols in seasonal climate forecasting over SA. All three experiments used the same set of aerosol emissions (Table S1 in SI), except for BB aerosols. The experiments were as follows: (1) BB emissions set to zero (BBZ), (2) monthly climatology (2003–2010) of BB emissions (BBC) derived from QFED, and (3) daily estimation of BB emissions (BBD) from QFED.BB emissions were utterly excluded in the BBZ experiment, and therefore, only aerosols from the other sources (Table S1 in SI) continue to act on radiation and cloud microphysics. Comparing the model results from these three experiments allows us to assess the impact of the BB aerosol forcing in the seasonal climate prediction and its sensitivity to the realism of the aerosol emissions.

Each hindcast consisted of a four-member ensemble produced from different initial atmospheric conditions. Every four members were initialized on 15, 20, 25, and 30 June, with the model running from June to November for each of the 16 years from 2000 to 2015, accounting for 6 months of integration, discarding June as spin-up period. Our analysis focused only on the August–October (ASO) season. Therefore, all average values presented hereinafter refer to the ASO months of the years from 2000 to 2015 over SA. For the aerosol analysis, we also focused on the area most directly affected by the smoke (Region 2; 15–5°S;70–50 W) and on the areas to the north (Region 1; 10°S–5°N;75–50 W) and south (Region 3; 35–15°S;70–50 W), to which the aerosols are transported (Figure 1a).

3. Results

Figures 1c–1e show the spatial distribution of AOD (550 nm) over SA for ASO derived from MERRA-2 and GEOS-S2S-2 model for BBC and BBD experiments. In both cases, the spatial distribution of predicted AOD showed good resemblance with MERRA-2. The simulations show higher AOD values in the central region of SA, which is directly related to BB aerosol emissions from local fires. GEOS-S2S-2 captured well the atmospheric circulation impact on the spatial distribution of AOD, typically noticed during the austral winter, such as BB aerosols transport from region 2 to southern and southeastern SA in association with the South Atlantic subtropical high (SASH) and the low-level jets (LLJ) circulation. Trade winds also contribute to transport aerosols to areas far away from the sources, such as Peru and Bolivia. Figure 1b shows a scatterplot of the annual ASO mean AOD values over SA from BBC and BBD experiments relative to MERRA-2. The biases were −0.04 and −0.03 for the BBC and BBD experiments, respectively, while the root-mean-square errors were 0.06 and 0.04. The use of climatological emissions was responsible for dropping the correlation coefficient (*R*) from 0.91 to 0.43. Although GOCART is interactive with the atmospheric conditions, the SA AOD prediction during the dry season is sensitive mostly to the BB emissions used. The high similarity between the climatological mean spatial distributions of AOD in the BBC and BBD experiments (Figures 1d and 1e), computed over the 2000–2015 period, may seem to contradict this statement. However, it should be noted that the AOD interannual variability predicted by each of these two experiments is remarkably different. The observed AOD annual variability from MERRA-2 is much better represented in BBD than on the BBC, as shown in Figure 1b.

There were also significant differences in the aerosol-induced changes in the radiative forcing over SA between BBC and BBD relative to BBZ experiments. The spatial distribution of the aerosol direct radiative
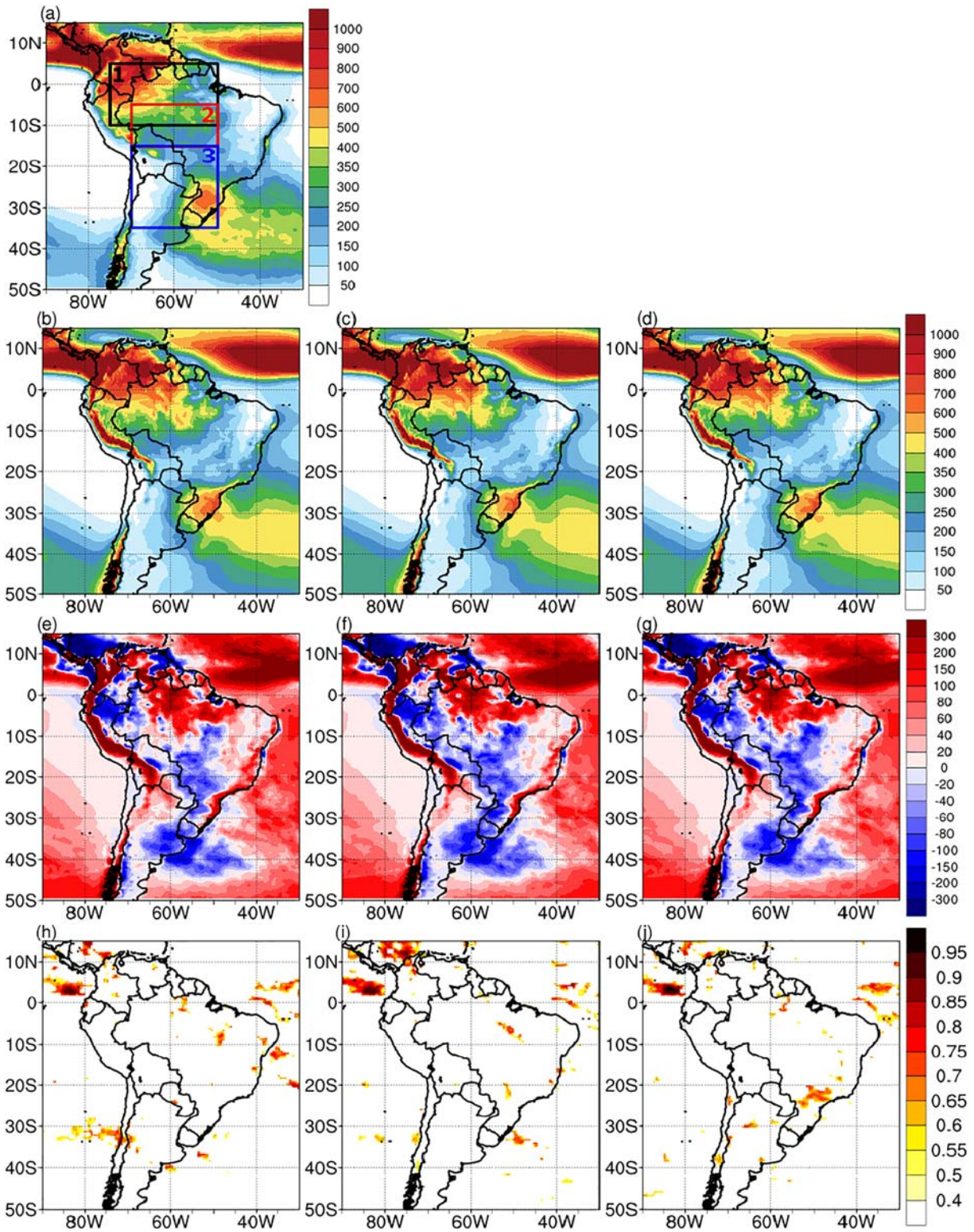
Figure 3. Climatological mean ASO spatial distribution (2000–2015) of precipitation (mm/day) from (a) TRMM, (b) BBZ, (c) BBC, and (d) BBD. Mean bias of precipitation from GEOS-S2S-2 relative to TRMM for (e) BBZ, (f) BBC, and (g) BBD experiments. Correlation between precipitation anomaly from GEOS-S2S-2 and the corresponding TRMM for (h) BBZ, (i) BBC, and (j) BBD experiments. The correlation plots show only the points with 5%SSL using a two-sided Student's *t* test.

Table 2
Correlation (R), Bias, and Mean Square Root Error (RMSE) for Precipitation (mm/day) Predicted Anomalies and TRMM Over the Regions 1–3 From All Three Experiments

|	Region 1 (10°S–5°N;75–50 W)			Region 2 (15–5°S;70–50 W)			Region 3 (35–15°S;65–45 W)		
	R	Bias	RMSE	R	Bias	RMSE	R	Bias	RMSE
BBZ	0.58	52	55	0.43	14	43	0.48	−8	51
BBC	0.61	50	55	0.58	−13	42	0.54	−21	51
BBD	0.56	52	56	0.52	−16	43	0.58	−19	50

Note. The regions are depicted in Figure 3a.

forcing (ADF; Figure S2 in SI) has the same shape as that of the AOD (Figure 1c). Inspecting region 2, which has the highest AOD values, the top of the atmosphere (TOA), surface (SUR), and the atmospheric (ATM) for clear-sky mean aerosol ADF averages, for both experiments BBD and BBC, were about −5, −17, and 11 Wm^{-2}, respectively (Table S2 in SI). These results agree with various observational and numerical studies investigating the role of BB aerosols in SA (Menezes Neto et al., 2017; Procopio et al., 2004; Thornhill et al., 2018).

In contrast to the direct forcing, the aerosol indirect radiative forcing (AIF) over SA has an almost bipolar spatial distribution (Figure S3 in SI), with a predominance of negative values at the north of latitude 10°S and positive values south of it. As predicted by the BBD experiment, the AIF ranged from about −10 to +10 Wm^{-2}, with mean values in regions 1–3 being −1.31 (±1.20), 0.25 (±1.37), and +1.23 (± 0.90) Wm^{-2}, respectively (Table S3 in SI). Over SA, the mean AIF was 0.5 (±1.60) Wm^{-2}. The use of climatological emissions tends to change the AIF signal from negative to positive in the region with the highest AOD (region 2; Figure 1a) while increasing its intensity elsewhere. Unlike the direct aerosol forcing, the indirect does not have a linear relationship with the BB emissions, which is somehow expected as it results from several competing processes.

Figures 2b–2d illustrate that the model reproduced the climatological 2-m temperature (T2M, °C) pattern over SA depicted by MERRA-2 (Figure 2a) for all three experiments, with the highest temperatures over the tropical region and with temperatures decreasing toward southern SA (Figure 2a). Including BB aerosols led to a reduction of T2M bias (Figures 2e and 2f), especially over areas with high aerosol loading. For region 1, the GEOS-S2S-2 system underestimated T2M for all experiments, and the mean bias values were −0.12°C, −0.19°C, and −0.17°C for BBZ, BBC, and BBD, respectively. Including BB aerosols did not contribute to reducing the bias of the near-surface temperature over region 1. On the other hand, in region 2, all experiments overestimated T2M relative to MERRA-2. The mean biases were 0.21°C, 0.04°C, and 0.07°C for BBZ, BBC, and BBD, respectively. In region 3, the BB aerosols also reduced the T2M biases, however, to a lower extent when compared to region 2. The mean bias values in region 3 were 0.08°C, −0.01°C, and −0.04°C for BBZ, BBC, and BBD, respectively. The mean RMSE was more pronounced for region 3, reaching up to 1.4°C (Table 1).

BB aerosols also positively impacted the correlation between T2M anomalies from the model predictions and MERRA-2. The shaded area below latitude 10°S in Figures 2i and 2j increased compared to Figure 2h. For the BBD experiment (Figure 2j), there is a noticeable increase in the correlation around 25°S and 50°W, which coincides with a local maximum climatological precipitation feature, as shown by TRMM (Figure 3a). On average, there was an improvement in the statistical metrics for the T2M of the BBC and BBD experiments compared to the BBZ experiment, mainly in regions 2 and 3 (Table 1).

The model reproduced the climatological precipitation pattern over SA during the ASO season, as depicted by TRMM (Figure 3a) for all three experiments (Figures 3b–3d). Most of the central SA region and the Northeast portion of Brazil presented much lower rainfall values than the extreme north sector of northern SA (Figure 3a). Including BB aerosols did not cause substantial precipitation changes, either for BBC or BBD, compared to the BBZ experiment (Figures 3b–3d). There was only a slight reduction in precipitation of about 10% and 5% in regions 2 and 3, respectively, barely noticeable in the plots. The precipitation suppression in BBC and BBD is consistent with the near-surface temperature reduction, the stabilization of the
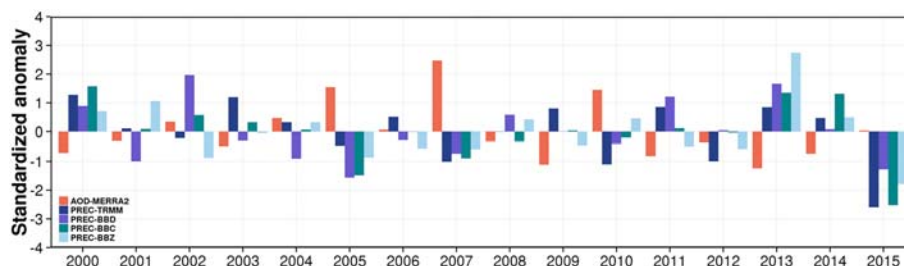
Figure 4. Standardized accumulated precipitation anomaly for the three model experiments and TRMM for ASO for the period from 2000 to 2015, over the region 2. Also, the standardized AOD anomaly from MERRA-2 is shown.

PBL, and the weakening of the upward motion at the lower troposphere (not shown). However, it does not translate into a reduction of either bias (Figures 3e–3g) or RMSE (Table 2). The mean precipitation bias over regions 2 and 3 changed from 14 to −16 for BBZ and from −8 to −19 for BBD. Regarding the correlation between the precipitation anomalies from the model and TRMM, there are very few spots with statistical significance correlations at the 5% level (5%SSL) all over SA and surrounded oceanic areas for all three experiments (Figures 3h–3j). This illustrates the challenge of predicting the location and time evolution of precipitation, even when the spatial distribution pattern is well represented. Still, the correlation index for the BBD experiment increased, relative to all the other experiments, over a small area, which coincides with a local maximum climatological precipitation feature between latitudes 20°S and 25°S (Figure 3j), which likely related to a better representation of the circulation pattern (not shown).

Figure 4 illustrates the mean interannual variability of the standardized accumulated precipitation anomaly for ASO from 2000 to 2015 for the three experiments and the TRMM data set over region 2. Figure 4 also shows the standardized AOD anomaly from MERRA-2 over that same region. In most years, there was a negative association between precipitation and AOD anomalies. The years 2005, 2007, 2010, and 2015 had the most significant rainfall deficit and positive AOD anomalies, with the precipitation anomalies above 1σ (where σ is the climatological standard deviation of the ASO seasonal mean). Except for 2005, during these years, BBC and BBD experiments, which included BB aerosol forcing, achieved better performance than the BBZ experiment.

On the other hand, the years 2000, 2009, 2011, and 2013 have positive precipitation anomalies, with the climatological standard deviation of the ASO seasonal mean close to 1σ, and negative AOD anomalies. However, for 2000 and 2013, the precipitation anomalies predicted by the three experiments have the same sign as the observation. For 2011, the anomaly was of the opposite sign only for BBZ. For 2009, the anomalies for BBC and BBD experiments were very close to zero but still positive, as the anomaly from TRMM, while for BBZ, the anomaly was not only negative but also further from zero. Despite some caveats, overall, the precipitation predicted by the BBC and BBD experiments achieved better performance than the BBZ experiment.

4. Conclusions

The ASO seasonal prediction of the spatial climatological distribution of AOD (550 nm) over SA was hardly sensitive to the use of climatological (BBC) or daily (BBD) emissions. However, the BBC experiment failed to reproduce the interannual variability of AOD depicted by MERRA-2.

The ADF mostly affected the area with higher BB aerosol loading (region 2), while the AIF was negative north of region 2 and positive elsewhere. Using climatological emissions increased the ADF in the atmosphere and reduced near-surface and on top of the atmosphere, while changed the AIF signal from negative to positive in region 2.

Including BB aerosols, in general, improved the prediction of atmospheric variables climatological patterns of atmospheric variables, such as T2M. The results of BBC and BBD experiments were closer to MERRA-2

reanalysis than the BBZ experiment, enhancing the correlation between the predicted and observed T2M anomalies and reducing bias and RMSE.

BB aerosols suppressed precipitation predictions over SA, especially in the region near the emission sources (region 2) and along with the smoke transport southward (regions 3). Our understanding is that the suppression occurred through two main mechanisms. First, the BB aerosol cooled the near-surface atmosphere, increasing the stability in the PBL, and limiting the convective development, which in turn suppresses cloud formation. Second, with the near-surface temperature reduction, the surface pressure increased, and the LLJ intensified. Nevertheless consistent, the improvement in predicting the atmospheric dynamical behavior did not impact precipitation prediction performance at the same degree. During the dry season, the atmospheric circulation determines very low precipitation rates in most SA, except in the northern and southern parts of the continent. In the region with the highest BB aerosol loading, where the atmospheric thermodynamic is mostly affected by them, it rains very little. Therefore, it is not easy to measure the impact of aerosols on precipitation prediction performance because it does not rain significantly. The correlation between the precipitation anomalies predicted by the model and estimated using TRMM data was sparse, with very few spots with 5% SSL all over SA and surrounded oceanic areas, almost equally for all three experiments performed. These results suggest that including aerosol forcing, even for extreme cases such as BB, does not eliminate the need to increase the model spatial resolution to predict the location and time evolution of precipitation accurately. Nevertheless, there was an enhancement of the precipitation prediction performance for the BBD experiment in one small area, affected by long-range BB aerosol transport, over a local climatological precipitation maximum depicted by TRMM, likely due to a better representation of the circulation pattern.

Our results highlighted yet a negative association between precipitation and the aerosol loading, that is, positive precipitation anomalies are consistent with negative AOD anomalies of BB aerosols and vice versa, as previously reported by Coelho et al. (2012). This relationship was even more evident for years of climatic extremes, such as when ENSO was active.

Using more realistic BB emissions, accurately representing the annual variability, instead of climatological BB emissions, improved the model representation of the ASO seasonal climate over SA. As climate models have increasingly been including more sophisticated aerosol treatments, it is crucial to also move toward a better representation of aerosol emissions. In particular, for SA, it is essential to develop prediction capability for vegetation fires and associated BB aerosol emissions on a seasonal scale.

Data Availability Statement

FAIR data standards data availability: GEOS S2S data is available at https://gmao.gsfc.nasa.gov/gmaoftp/2020GL088096R/GEOS-S2S/ website. The file specification document that elaborates on the available output from GEOS-S2S is available from https://gmao.gsfc.nasa.gov/pubs/docs/Nakada1033.pdf website. The MERRA-2 Reanalysis, the TRMM precipitation data, and the QFED emissions products were downloaded, respectively, from https://gmao.gsfc.nasa.gov/reanalysis/MERRA-2/data_access/, https://pmm.nasa.gov/data-access/downloads/trmm, and https://portal.nccs.nasa.gov/datashare/iesa/aerosol/emissions/QFED/v2.5r1/0.25/QFED/ websites.

References

Allen, R. J., Sherwood, S. C., Norris, J. R., & Zender, C. S. (2012). Recent Northern Hemisphere tropical expansion primarily driven by black carbon and tropospheric ozone. *Nature*, *485*(7398), 350–354. https://doi.org/10.1038/nature11097

Allen, R. J., Sherwood, S. C., Norris, J. R., & Zender, C. S. (2012a). The equilibrium response to idealized thermal forcings in a comprehensive GCM: Implications for recent tropical expansion. *Atmospheric Chemistry and Physics*, *12*(10), 4795–4816. https://doi.org/10.5194/acp-12-4795-2012

Andrews, T., Forster, P. M., & Gregory, J. M. (2009). A surface energy perspective on climate change. *Journal of Climate*, *22*(10), 2557–2570. https://doi.org/10.1175/2008JCLI2759.1

Barahona, D., Molod, A., Bacmeister, J., Nenes, A., Gettelman, A., Morrison, H., et al. (2014). Development of two-moment cloud microphysics for liquid and ice within the NASA Goddard Earth Observing System Model (GEOS-5). *Geoscientific Model Development*, *7*, 1733–1766. https://doi.org/10.5194/gmd-7-1733-2014

Barahona, D., & Nenes, A. (2008). Parameterization of cirrus formation in large scale models: Homogeneous nucleation. *Journal of Geophysical Research*, *113*, D11211. https://doi.org/10.1029/2007JD009355

Barahona, D., & Nenes, A. (2009). Parameterizing the competition between homogeneous and heterogeneous freezing in cirrus cloud formation—Monodisperse ice nuclei. *Atmospheric Chemistry and Physics*, *9*, 369–381. https://doi.org/10.5194/acp-9-369-2009

Benedetti, A., & Vitart, F. (2018). Can the direct effect of aerosols improve subseasonal predictability? *Monthly Weather Review*, *146*(10), 3481–3498. https://doi.org/10.1175/MWR-D-17-0282.1

Chou, M.-D. (1990). Parameterizations for the absorption of solar radiation by O_2 and CO_2 with applications to climate studies. *Journal of Climate*, *3*(2), 209–217. https://doi.org/10.1175/1520-0442(1990)003<0209:PFTAOS>2.0.CO;2

Chou, M.-D. (1992). A solar radiation model for use in climate studies. *Journal of the Atmospheric Sciences*, *49*(9), 762–772. https://doi.org/10.1175/1520-0469(1992)049<0762:ASRMFU>2.0.CO;2

Chou, M.-D., & Suarez, M. J. (1994). An efficient thermal infrared radiation parameterization for use in general circulation models, *NASA Tech. Memorandum*, NASA/TM- 1994-104606, Vol. 3, 85 pp.

Coelho, C. A., Cavalcanti, I. A., Costa, S. M., Freitas, S. R., Ito, E. R., Luz, G., et al. (2012). Climate diagnostics of three major drought events in the Amazon and illustrations of their seasonal precipitation predictions. *Meteorological Applications*, *19*(2), 237–255. https://doi.org/10.1002/met.1324

Darmenov, A., & da Silva, A. (2015). The quick fire emissions dataset (QFED)—Documentation of versions 2.1, 2.2 and 2.4. *Technical Report Series on Global Modeling and Data Assimilation*. URL http://gmao.gsfc.nasa.gov/pubs/docs/Darmenov796.pdf

Doblas-Reyes, F. J., García-Serrano, J., Lienert, F., Biescas, A. P., & Rodrigues, L. R. (2013). Seasonal climate predictability and forecasting: Status and prospects. *Wiley Interdisciplinary Reviews: Climate Change*, *4*(4), 245–268. https://doi.org/10.1002/wcc.217

Fountoukis, C., & Nenes, A. (2005). Continued development of a cloud droplet formation parameterization for global climate models. *Journal of Geophysical Research*, *110*, D11212. https://doi.org/10.1029/2004JD005591

Gácita, M. S., Longo, K. M., Freire, J. L., Freitas, S. R., & Martin, S. T. (2017). Impact of mixing state and hygroscopicity on CCN activity of biomass burning aerosol in Amazonia. *Atmospheric Chemistry and Physics*, *17*(3). https://doi.org/10.5194/acp-17-2373-2017

Gelaro, R., McCarty, W., Suárez, M. J., Todling, R., Molod, A., Takacs, L., et al. (2017). The modern-era retrospective analysis for research and applications, version 2 (MERRA-2). *Journal of Climate*, *30*(14), 5419–5454. https://doi.org/10.1175/JCLI-D-16-0758.1

He, J., & Soden, B. J. (2015). Anthropogenic weakening of the tropical circulation: The relative roles of direct CO_2 forcing and sea surface temperature change. *Journal of Climate*, *28*(22), 8728–8742. https://doi.org/10.1175/JCLI-D-15-0205.1

Kirtman, B., & Pirani, A. (2009). The state of the art of seasonal prediction: Outcomes and recommendations from the first world climate research program workshop on seasonal prediction. *Bulletin of the American Meteorological Society*, *90*(4), 455–458. https://doi.org/10.1175/2008BAMS2707.1

Koop, T., Luo, B., Tsias, A., & Peter, T. (2000). Water activity as the determinant for homogeneous ice nucleation in aqueous solutions. *Nature*, *406*(6796), 611–614. https://doi.org/10.1038/35020537

Li, X., Ting, M., You, Y., Lee, D. E., Westervelt, D. M., & Ming, Y. (2020). South Asian summer monsoon response to aerosol-forced sea surface temperatures. *Geophysical Research Letters*, *47*, e2019GL085329. https://doi.org/10.1029/2019gl085329

Ma, J., & Xie, S. P. (2013). Regional patterns of sea surface temperature change: A source of uncertainty in future projections of precipitation and atmospheric circulation. *Journal of Climate*, *26*(8), 2482–2501. https://doi.org/10.1175/JCLI-D-12-00283.1

Menezes Neto, O. L., Coutinho, M. M., Marengo, J. A., & Capistrano, V. B. (2017). The impacts of a plume-rise scheme on earth system modeling: Climatological effects of biomass aerosols on the surface temperature and energy budget of South America. *Theoretical and Applied Climatology*, *129*(3–4), 1035–1044. https://doi.org/10.1007/s00704-016-1821-y

Molod, A., Hackert, E., Vikhliaev, Y., Zhao, B., Barahona, D., Vernieres, G., et al. (2020). GEOS-S2S Version 2: The GMAO high resolution coupled model and assimilation system for seasonal prediction. *Journal of Geophysical Research: Atmospheres*, *125*, e2019JD031767. https://doi.org/10.1029/2019jd031767

Nenes, A., & Seinfeld, J. H. (2003). Parameterization of cloud droplet formation in global climate models. *Journal of Geophysical Research*, *108*(D14), 4415. https://doi.org/10.1029/2002JD002911

Phillips, V. T., Demott, P. J., Andronache, C., Pratt, K. A., Prather, K. A., Subramanian, R., & Twohy, C. (2013). Improvements to an empirical parameterization of heterogeneous ice nucleation and its comparison with observations. *Journal of the Atmospheric Sciences*, *70*(2), 378–409. https://doi.org/10.1175/JAS-D-12-080.1

Procopio, A. S., Artaxo, P., Kaufman, Y. J., Remer, L. A., Schafer, J. S., & Holben, B. N. (2004). Multiyear analysis of Amazonian biomass burning smoke radiative forcing of climate. *Geophysical Research Letters*, *31*, L03108. https://doi.org/10.1029/2003GL018646

Randles, C. A., Colarco, P. R., & Da Silva, A. (2013). Direct and semi-direct aerosol effects in the NASA GEOS-5 AGCM: Aerosol-climate interactions due to prognostic versus prescribed aerosols. *Journal of Geophysical Research: Atmospheres*, *118*, 149–169. https://doi.org/10.1029/2012JD018388

Randles, C. A., Da Silva, A. M., Buchard, V., Colarco, P. R., Darmenov, A., Govindaraju, R., et al. (2017). The MERRA-2 aerosol reanalysis, 1980 onward. Part I: System description and data assimilation evaluation. *Journal of Climate*, *30*(17), 6823–6850. https://doi.org/10.1175/JCLI-D-16-0609.1

Rosário, N. E. D., Longo, K. M., Freitas, S. R. D., Yamasoe, M. A., & Fonseca, R. M. D. (2013). Modeling the South American regional smoke plume: Aerosol optical depth variability and surface shortwave flux perturbation. *Atmospheric Chemistry and Physics*, *13*(6), 2923–2938. https://doi.org/10.5194/acp-13-2923-2013

Simpson, J., Kummerow, C., Tao, W. K., & Adler, R. F. (1996). On the tropical rainfall measuring mission (TRMM). *Meteorology and Atmospheric Physics*, *60*(1–3), 19–36. https://doi.org/10.1007/BF01029783

Thornhill, G. D., Ryder, C. L., Highwood, E. J., Shaffrey, L. C., & Johnson, B. T. (2018). The effect of South American biomass burning aerosol emissions on the regional climate. *Atmospheric Chemistry and Physics*, *18*(8), 5321–5342. https://doi.org/10.5194/acp-18-5321-2018

Tosca, M. G., Randerson, J. T., & Zender, C. S. (2013). Global impact of smoke aerosols from landscape fires on climate and the Hadley circulation. *Atmospheric Chemistry and Physics*, *13*, 5227–5241. https://doi.org/10.5194/acp-13-5227-2013

Wang, Y., Ma, P. L., Jiang, J. H., Su, H., & Rasch, P. J. (2016). Toward reconciling the influence of atmospheric aerosols and greenhouse gases on light precipitation changes in Eastern China. *Journal of Geophysical Research: Atmospheres*, *121*, 5878–5887. https://doi.org/10.1002/2016JD024845

Yu, H., Liu, S. C., & Dickinson, R. E. (2002). Radiative effects of aerosols on the evolution of the atmospheric boundary layer. *Journal of Geophysical Research*, *107*(D12) AAC-3, 4142. https://doi.org/10.1029/2001JD000754

References From the Supporting Information

Bey, I., Jacob, D. J., Yantosca, R. M., Logan, J. A., Field, B. D., Fiore, A. M., et al. (2001). Global modeling of tropospheric chemistry with assimilated meteorology: Model description and evaluation. *Journal of Geophysical Research*, *106*(D19), 23,073–23,095. https://doi.org/10.1029/2001JD000807

Bosilovich, M. G. (2015). MERRA-2: Initial evaluation of the climate. *NASA Technical Report Series on Global Modeling and Data Assimilation*, v. 43, n. September

Chin, M., Ginoux, P., Kinne, S., Torres, O., Holben, B. N., Duncan, B. N., et al. (2002). Tropospheric aerosol optical thickness from the GOCART model and comparisons with satellite and Sun photometer measurements. *Journal of the Atmospheric Sciences*, *59*, 461–483. https://doi.org/10.1175/1520-0469

Colarco, P., da Silva, A., Chin, M., & Diehl, T. (2010). Online simulations of global aerosol distributions in the NASA GEOS-4 model and comparisons to satellite and ground-based aerosol optical depth. *Journal of Geophysical Research*, *115*, D14207. https://doi.org/10.1029/2009JD012820

COMMISSION, E. (2011). European Commission/Joint Research Centre (JRC)/Netherlands Environmental Assessment agency (PBL): Emission Database For Global Atmospheric Research (EDGAR), release version 4.1. URL http://edgar.jrc.ec.europa.eu>

Diehl, T., Heil, A., Chin, M., Pan, X., Streets, D., Schultz, M., & Kinne, S. (2012). Anthropogenic, biomass burning, and volcanic emissions of black carbon, organic carbon, and SO 2 from 1980 to 2010 for hindcast model experiments. *Atmospheric Chemistry and Physics Discussions*, *12*(9), 24,895–24,954. https://doi.org/10.5194/acpd-12-24895-2012

Ginoux, P., Chin, M., Tegen, I., Prospero, J. M., Holben, B., Dubovik, O., & Lin, S. J. (2001). Sources and distributions of dust aerosols simulated with the GOCART model. *Journal of Geophysical Research*, *106*(D17), 20,255–20,273. https://doi.org/10.1029/2000JD000053

Gong, S. L. (2003). A parameterization of sea-salt aerosol source function for sub- and super-micron particles. *Global Biogeochemical Cycles*, *17*(4), 1097. https://doi.org/10.1029/2003GB002079

Griffies, S. (2012). Elements of the modular ocean model (MOM). http://mdl-mom5. herokuapp.com/web/docs/project/MOM5_elements. pdf

Griffies, S. M., Gnanadesikan, A., Dixon, K. W., Dunne, J. P., Gerdes, R., Harrison, M. J., et al. (2005). Formulation of an ocean model for global climate simulations. *Ocean Science*, *1*, 1025–1035. https://doi.org/10.5194/os-1-45-2005

Guenther, A., Hewitt, C. N., Erickson, D., Fall, R., Geron, C., Graedel, T., et al. (1995). A global model of natural volatile organic compound emissions. *Journal of Geophysical Research*, *100*(D5), 8873–8892. https://doi.org/10.1029/94JD02950

Hill, C., DeLuca, C., Balaji, V., Suarez, M., & da Silva, A. (2004). Architecture of the earth system modeling framework. *Computing in Science & Engineering*, *6*, 1. https://doi.org/10.1109/MCISE.2004.1255817

Huffman, G. J., Bolvin, D. T., Nelkin, E. J., Wolff, D. B., Adler, R. F., Gu, G., et al. (2007). The TRMM multisatellite precipitation analysis (TMPA): Quasi-global, multiyear, combined-sensor precipitation estimates at fine scales. *Journal of Hydrometeorology*, *8*(1), 38–55. https://doi.org/10.1175/JHM560.1

Hunke, E., & Lipscomb, W. (2008). The Los Alamos sea ice model, documentation and software manual, version 4.0. *Technical report, Los Alamos National Laboratory*.

Jaeglé, L., Quinn, P. K., Bates, T. S., Alexander, B., & Lin, J. T. (2011). Global distribution of sea salt aerosols: New constraints from in situ and remote sensing observations. *Atmospheric Chemistry and Physics*, *11*(7), 3137–3157. https://doi.org/10.5194/acp-11-3137-2011

Kleist, D. T., Parrish, D. F., Derber, J. C., Treadon, R., Wu, W. S., & Lord, S. (2009). Introduction of the GSI into the NCEP global data assimilation system. *Weather and Forecasting*, *24*(6), 1691–1705. https://doi.org/10.1175/2009WAF2222201.1

Koster, R. D., Suarez, M. J., Ducharne, A., Stieglitz, M., & Kumar, P. (2000). A catchment-based approach to modeling land surface processes in a general circulation model: 1. Model structure. *Journal of Geophysical Research*, *105*(D20), 24,809–24,822. https://doi.org/10.1029/2000JD900327

Lana, A., Bell, T. G., Simó, R., Vallina, S. M., Ballabrera-Poy, J., Kettle, A. J., et al. (2011). An updated climatology of surface dimethlysulfide concentrations and emission fluxes in the global ocean. *Global Biogeochemical Cycles*, *25*, GB1004. https://doi.org/10.1029/2010GB003850

Lin, S.-J. (2004). A vertically Lagrangian finite-volume dynamical core for global models. *Monthly Weather Review*, *132*(10), 2293–2307. https://doi.org/10.1175/1520-0493(2004)132<2293:AVLFDC>2.0.CO;2

Lock, A. P., Brown, A. R., Bush, M. R., Martin, G. M., & Smith, R. N. B. (2000). A new boundary layer mixing scheme. Part I: Scheme description and single-column model tests. *Monthly Weather Review*, *138*, 3187–3199. https://doi.org/10.1175/1520-0493(2000)128<3187:anblms>2.0.co;2

Louis, J., & Geleyn, J. (1982). A short history of the PBL parameterization at ECMWF. In *Proc. ECMWF Workshop on Planetary Boundary Layer Parameterization, Reading* (pp. 59–80). United Kingdom: ECMWF.

Molod, A., Takacs, L., Suarez, M., & Bacmeister, J. (2015). Development of the GEOS-5 atmospheric general circulation model: Evolution from MERRA to MERRA2. *Geoscientific Model Development*, *8*, 1339–1356. https://doi.org/10.5194/gmd-8-1339-2015

Moorthi, S., & Suarez, M. J. (1992). Relaxed Arakawa Schubert: A parameterization of moist convection for general circulation models. *Monthly Weather Review*, *120*(6), 978–1002. https://doi.org/10.1175/1520-0493(1992)120<0978:RASAPO>2.0.CO;2

Putman, W. M., & Lin, S.-J. (2007). Finite-volume transport on various cubed-sphere grids. *Journal of Computational Physics*, *227*, 55–78. https://doi.org/10.1016/j.jcp.2007.07.022

Reichle, R. H., & Liu, Q. (2014). Observation-corrected precipitation estimates in GEOS-5. Technical Report Series on Global Modelling and Data Assimilation, Vol. 35, *NASA Tech. Rep. NASA/TM–2014–104606, 24 pp*. [Available online at https://ntrs.nasa.gov/archive/nasa/casi.ntrs.nasa.gov/20150000725.pdf.]

Rienecker, M. M., Suarez, M. J., Todling, R., Bacmeister, J., Takacs, L., Liu, H. C., et al. (2008). The GEOS-5 Data Assimilation System: Documentation of versions 5.0.1 and 5.1.0, and 5.2.0, NASA Tech. Rep. Series on Global Modeling and Data Assimilation, NASA/TM-2008-104606, Vol. 27, 92 pp.

Wu, W. S., Purser, R. J., & Parrish, D. F. (2002). Three-dimensional variational analysis with spatially inhomogeneous covariances. *Monthly Weather Review*, *130*(12), 2905–2916. https://doi.org/10.1175/1520-0493(2002)130<2905:TDVAWS>2.0.CO;2